Structural Changes of eIF4E upon Binding to the mRNA 5′ Monomethylguanosine and Trimethylguanosine Cap[†]

Izabela Rutkowska-Wlodarczyk,[‡,§] Janusz Stepinski,[||] Michal Dadlez,[‡,⊥] Edward Darzynkiewicz,[||] Ryszard Stolarski,[||] and Anna Niedzwiecka*[,§,||]

Institute of Biochemistry and Biophysics, Polish Academy of Sciences, 02-106 Warsaw, Poland, Biological Physics Group, Institute of Physics, Polish Academy of Sciences, 02-668 Warsaw, Poland, Division of Biophysics, Institute of Experimental Physics, Faculty of Physics, Warsaw University, 02-089 Warsaw, Poland, and Institute of Genetics and Biotechnology, Faculty of Biology, Warsaw University, 02-089 Warsaw, Poland

Received June 13, 2007; Revised Manuscript Received October 23, 2007

ABSTRACT: Recognition of the 5′ cap by the eukaryotic initiation factor 4E (eIF4E) is the rate-limiting step in the ribosome recruitment to mRNAs. The regular cap consists of 7-monomethylguanosine (MMG) linked by a 5′−5′ triphosphate bridge to the first transcribed nucleoside, while some primitive eukaryotes possess a N^2,N^2,7-trimethylguanosine (TMG) cap structure as a result of *trans* splicing. Mammalian eIF4E is highly specific to the MMG form of the cap in terms of association constants and thermodynamic driving force. We have investigated conformational changes of eIF4E induced by interaction with two cap analogues, 7-methyl-GTP and N^2,N^2,7-trimethyl-GTP. Hydrogen–deuterium exchange and electrospray mass spectrometry were applied to probe local dynamics of murine eIF4E in the *apo* and cap-bound forms. The data show that the cap binding induces long-range conformational changes in the protein, not only in the cap-binding pocket but also in a distant region of the 4E-BP/eIF4G binding site. Formation of the complex with 7-methyl-GTP makes the eIF4E structure more compact, while binding of N^2,N^2,7-trimethyl-GTP leads to higher solvent accessibility of the protein backbone in comparison with the *apo* form. The results suggest that the additional double methylation at the N^2-amino group of the cap causes sterical effects upon binding to mammalian eIF4E which influence the overall solution dynamics of the protein, thus precluding formation of a tight complex.

A complicated process of eukaryotic mRNA translation initiation involves formation of a large protein−RNA complex that directs the ribosome to the initiation codon. Canonical cap-dependent translation begins with specific recognition of the mRNA 5′-terminal monomethylguanosine cap [MMG-cap, 7-methylG(5′)ppp(5′)N, where N = G, A, U, or C] by the eukaryotic translation initiation factor eIF4E,[1] the smallest (25 kDa) component of a large eIF4F multiprotein complex (*1, 2*). The 5′ terminus of most nematode mRNAs, e.g., those in *Caenorhabditis elegans*, contains a trimethylguanosine cap structure, TMG-cap, with two additional methyl groups at N^2, $m_3^{2,2,7}$G(5′)ppp(5′)N (*3*). Both the TMG-cap and MMG-cap are recognized by some of the nematode eIF4E isoforms (*4, 5*), while the affinity of the hypermethylated cap analogues for mammalian eIF4E factors is 2−3 orders of magnitude lower than that of the MMG-cap (*6*). Binding of the MMG-cap to murine eIF4E is highly enthalpy-driven and entropy-opposed, while formation of the complex with $m_3^{2,2,7}$GTP is accompanied by a weak negative enthalpy change but a strong positive entropy change at 20 °C (*7*).

eIF4E is the least abundant initiation factor in most of the cell types (*8*), and its accessibility is thought to limit the efficiency of the overall ribosome recruitment to mRNA (*9*). A crucial role of eIF4E in translation initiation makes it a target for several regulating processes, including phosphorylation (*10, 11*) and suppression by eIF4E-binding proteins, 4E-BPs (*12*). A fragment of 4E-BP1 competes with the eIF4G scaffolding protein (*13*), the second component of the initiation eIF4F complex, for the same binding site at the dorsal surface of eIF4E, on the opposite side of the protein in relation to the cap-binding center (*14*). Structures of various mammalian and yeast eIF4Es bound to cap analogues were determined by X-ray crystallography (*6, 15, 16*) and multidimensional NMR (*17*), respectively. Crystal structures were also resolved for ternary complexes of mammalian eIF4E

[†] This research was supported by the Polish Ministry of Science and Higher Education, Grant 2 P04A 033 28, BST-1124/BF, 0445/P04/2005/29, and by the Howard Hughes Medical Institute, Grant 55005604 (to E.D.).

* Address correspondence to this author at the Polish Academy of Sciences. E-mail: annan@ifpan.edu.pl. Tel: (+48 22) 843 66 01 ext 3516. Fax: (+48 22) 843 09 26.

[‡] Institute of Biochemistry and Biophysics, Polish Academy of Sciences.

[§] Institute of Physics, Polish Academy of Sciences.

[||] Institute of Experimental Physics, Faculty of Physics, Warsaw University.

[⊥] Institute of Genetics and Biotechnology, Faculty of Biology, Warsaw University.

[1] Abbreviations: eIF4E, eukaryotic initiation factor 4E; m^7G, 7-methylguanosine; m^7GDP, 7-methylguanosine 5′-diphosphate; m^7GTP, 7-methylguanosine 5′-triphosphate; $m_3^{2,2,7}$GTP, N^2,N^2,7-trimethylguanosine 5′-triphosphate; HDE, hydrogen–deuterium exchange; MS, mass spectrometry; ESI-MS, electrospray ionization mass spectrometry; LC, liquid chromatography; HPLC, high-performance liquid chromatography; HEPES, *N*-(2-hydroxyethyl)-piperazine-*N*′-2-ethanesulfonic acid.

10.1021/bi701168z CCC: $40.75
Published on Web 01/26/2008

bound to a cap analogue and to a peptide mimicking the eIF4E recognition motif of either eIF4GII or 4E-BP1 (*14, 18*).

Without any bound ligand, eIF4E was found to be unstable and prone to aggregation (*6, 19*). The first evidence of a high flexibility of the *apo*-eIF4E and of significant conformational changes leading to stiffening of its structure upon binding to specific ligands came from thermodynamic studies that revealed a nontrivial isothermal enthalpy–entropy compensation for the 5′ cap analogue series (*7*). Then, a disorder-to-order transition upon m^7GDP binding was shown for yeast eIF4E by NMR (*20*), but the actual regions of induced folding still remain to be defined. Structural and dynamic consequences of m^7GDP binding were recently elucidated by the solution structure of *apo*-eIF4E, resolved by NMR (*21*). The authors showed a concerted hinge lock mechanism involving the W102 and W56 containing regions responsible for cation$-\pi$ stacking with the m^7G moiety and ligand-induced conformational rearrangements close to R157 and K159 that are engaged in binding of the phosphate chain. Some changes of the local dynamics and electrostatic charge distribution were also found in the dorsal eIF4G/4E-BP binding site. However, most of current conclusions were based on comparison of the 3D solution structures of *apo*-eIF4E (*21*) with the crystal structures of eIF4E−cap complexes (*6, 15, 16*). Our work is focused on direct analysis of structural changes of eIF4E upon binding to the MMG and TMG cap structures in solution within the same methodological assay.

Mass spectrometry (MS) has become an indispensable technique in proteomic research (*22, 23*) bringing us closer to understanding protein functions. One of the methods used to follow protein dynamics and their structural features is mass spectrometry coupled with hydrogen–deuterium exchange (HDE) (*24–28*). HDE-MS was successfully applied to determine protein–protein (*29–32*) and protein–ligand interactions (*33, 34*). This technique allows to perform experiments at low protein concentrations and to obtain structural information on those targets for which application of methods like NMR and/or X-ray crystallography are difficult. For these reasons HDE-MS seems to be a method of choice for studies of eIF4E conformational changes.

The aim of this work was to reveal differences in the eIF4E local structural stability due to the binding of two forms of the cap and to check whether interactions within the cap-binding slot could induce nonlocal conformational changes, especially in the eIF4E dorsal surface recognized by the 4E-BP inhibitory proteins and the eIF4G translation factor (*14*). We present structural consequences of binding of synthetic cap analogues to murine eIF4E, monitored by HDE-MS. The sequence-specific information was derived from kinetics of the amide protons exchange for deuterons, followed by the MS analysis of the protein fragments after pepsin cleavage. We determined a correlation between the affinities of the cap analogues to eIF4E and localized conformational changes of the protein caused by the interaction. Following NMR and X-ray crystallography techniques, the HDE experiments provide a complementary structural insight into the submolecular mechanism of eIF4E activity upon eukaryotic translation initiation.

Scheme 1: Chemical Structures of the Cap Analogues, the Monomethylguanosine Cap Analogue, m^7GTP (R = H), and the Trimethylguanosine Cap Analogue, $m_3^{2,2,7}$GTP (R = CH_3)

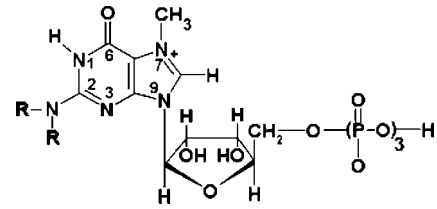

MATERIALS AND METHODS

Cap Analogues, Proteins, and Reagents. m^7GTP and $m_3^{2,2,7}$GTP (Scheme 1) were synthesized as reported previously (*35, 36*). Murine eukaryotic initiation factor eIF4E (residues 28–217) was expressed in *Escherichia coli* (*37*) and purified from inclusion bodies without any contact with cap analogues as described previously (*6*). The protein was filtered through Biomax 100K NMWL (Millipore) before each experiment. Deuterium oxide (99.8%) was purchased from Armar AG (Switzerland) and pepsin from ICN (Germany).

Isotope Labeling. $^1H-^2H$ exchange (in-exchange) was performed in a 20 μM solution of eIF4E (28–217) in 50 mM HEPES, pH 7.0, and 200 mM KCl, either in the *apo* form or in the complexes with a cap analogue (30 μM m^7GTP or 7 mM $m_3^{2,2,7}$GTP, to ensure 99% saturation, based on the association constants (*6*)), by 10-fold dilution in ^2H_2O and incubation on ice for increasing periods of 15 s to 10 min. The exchange was terminated by acidification with formic acid to a p^{2}H value of 2.8–3.0, calculated by means of a SPHERE program (*38*) which took into account a consecutive sequence of the amino acid pairs in a protein sequence and calculated the pH value of the slowest exchange rate of each specific amide hydrogen. The average of the pH values calculated for all amino acid pairs in eIF4E was applied in our HDE experiments. The temperature at the termination step of the exchange was shifted to 10 °C.

The protein samples were either directly analyzed by MS or subjected to pepsin digestion (1:1 enzyme-to-protein ratio), at p^{2}H 3.0, for 4 min at 10 °C. The peptide mixture was subsequently analyzed for deuterium incorporation by LC-MS and identified by LC-MS/MS (see below). To determine the peptide masses and to identify the nonexchanged peptides (control 1), the same protocol was used as in the in-exchange experiments, except for replacing ^2H_2O by H_2O. Another set of control samples of the fully exchanged eIF4E peptides (control 2) was prepared as follows. The protein was first digested with pepsin (1:1 protein-to-enzyme ratio) at 0 °C, pH 3, for 5 min, then diluted 10-fold in ^2H_2O at room temperature, p^{2}H 7, and incubated for 2 h to replace all exchangeable protons by deuterons.

Mass Spectrometry. The deuterium incorporation level in the undigested protein as well as in the pepsin-generated peptides was determined by mass spectrometry. The samples of the undigested protein were desalted for 5 min on a C4 precolumn and eluted with a linear gradient of acetonitrile, 0−70%, for 10 min (flow rate of 0.2 μL/min) directly to the ion source of the MS spectrometer by means of a nano-HPLC system (LC Packings). The samples containing peptides after pepsin digestion were desalted and fractionated on a C18 precolumn using the same acetonitrile gradient. A time lapse,

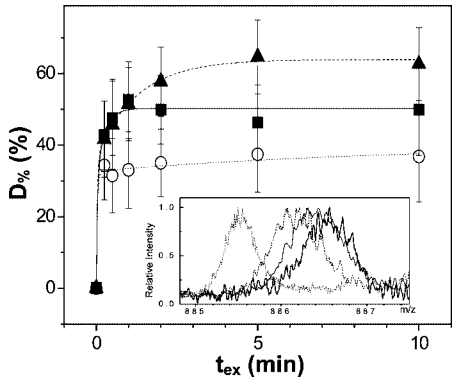

FIGURE 1: Comparison of deuteration level of the whole eIF4E in three forms. Kinetics of deuterium incorporation into the eIF4E−m^{7}GTP complex (open circles), *apo*-eIF4E (filled squares), and eIF4E−m$_3^{2,2,7}$GTP complex (filled triangles). Inset: Fragments of mass spectra corresponding to undeuterated eIF4E (dotted line) and after 10 min of hydrogen–deuterium exchange for the protein in the complex with m^{7}GTP (dashed line), *apo* form (solid line), and the complex with m$_3^{2,2,7}$GTP (thick solid line), at the eIF4E charge state of +25, uncorrected for back-exchange.

from adding of pepsin to loading of the sample on the nano-HPLC column, was kept constant for all samples and was limited by the autosampler procedure (4 min from "start" to sample loading). To minimize the loss of deuterium due to the back-exchange effect (*39, 40*), the buffers used to load the samples and to elute the peptides were adjusted to pH 2.8 and cooled to 4 °C. The autosampler plate was cooled to 10 °C. The eluate from the precolumn was directly injected to the spectrometer ion source.

Mass spectra were acquired on a Q-ToF1 ESI-MS spectrometer (Waters) in a positive ion mode, with a capillary voltage of 2.5 kV and a cone voltage of 35 V. The flow rates of the nebulizing gas and the drying gas were 20 and 450 L/h, respectively. The spectrometer worked either in the data-dependent MS to MS/MS mode for peptide identification or in the MS survey mode for the assessment of the deuterium incorporation. To improve sequence coverage, a LTQ-FT-MS spectrometer (Thermo), working in the MS/MS mode, was used instead of Q-ToF1, in a positive ion mode, with a capillary voltage of 1.5 kV and a cone voltage of 44 V. Acquired data were analyzed and visualized using in-house LC-MS data analysis software (Poznanski et al., to be published elsewhere).

Identification of Pepsin Cleavage Products. Identification of the nonexchanged peptides was carried out using the Mascot data search engine (*41*). The MS/MS raw data were processed by Mascot Distiller followed by Mascot Search (Matrix Science, London, U.K.) against the NCBI nonredundant database. Search parameters for precursor and product ion mass tolerance were 200 ppm and 0.4 Da, respectively, without a defined enzyme specificity (enzyme = "none") and without fixed modifications. Only methionine oxidation was allowed. The sequence and the HPLC retention time obtained in this way were stored in the Pepsin Peptides Database (PPD).

Unambiguous identification of peptides after HDE and pepsin cleavage was carried out by visual inspection of two overlaid 2D signal maps, i.e., the one for the nonexchanged sample with the identity tags assigned from PPD and the other for the exchanged sample (Figure 2G). In cases of doubt, a comparison of the fragmentation patterns of the

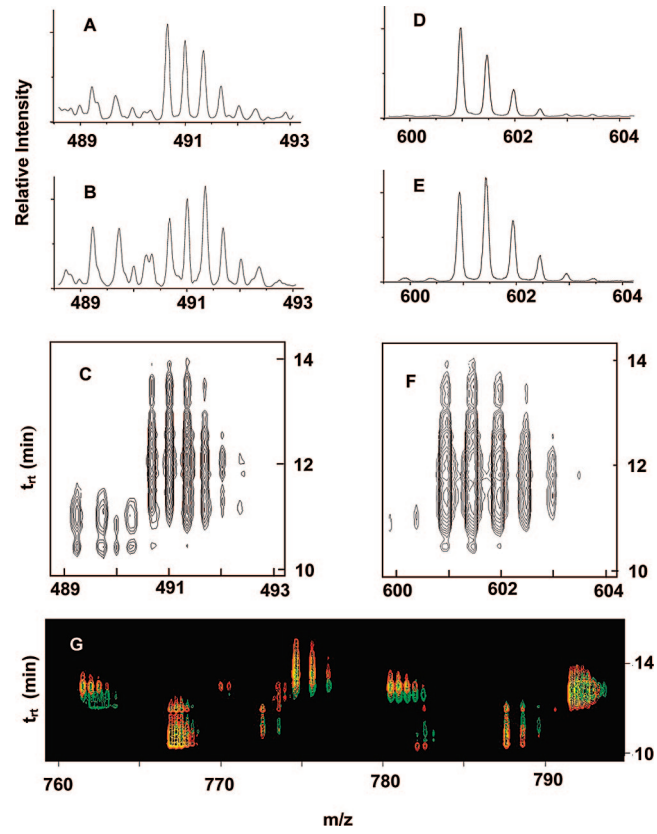

FIGURE 2: Examples of LC-MS analysis of peptic digestion of *apo*-eIF4E. (A) MS signal of the unexchanged ^{61}RLISKFDTVEDF^{72} peptide (m = 1468.7 Da, z = +3, retention time 10–14 min); (B) MS signal of the peptide after the complete hydrogen–deuterium exchange; (C) the corresponding 2D signal map. (D) MS signal of the unexchanged ^{63}ISKFDTVEDF^{72} peptide (m = 1199.6 Da, z = +2, retention time 10–14 min); (E) MS signal of the peptide after the complete HDE; (F) the corresponding 2D signal map. (G) Overlay of two 2D signal maps for unexchanged peptides (red) and the peptides after HDE (green).

signals arising from the exchanged and nonexchanged samples was sufficient to confirm or disprove the sequence identity.

Corrections for Back-Exchange. To estimate an approximate level of back-exchange of deuterons for protons for undigested eIF4E, the protein was denatured by 1 h at 60 °C in 10 mM ammonium acetate and 90% ^2H_2O, p^{2}H 7.0. Next, formic acid was added to a final p^{2}H of 3, and a fraction of the sample was manually injected directly to the spectrometer ion source. Another fraction of the same sample was loaded on a C4 precolumn and eluted with a similar as previously gradient of acetonitrile.

To determine the individual back-exchange level for each pepsin-generated peptide, a mixture of the fully exchanged peptides was subjected to LC-MS analysis with various additional delay times during the desalting step on the C18 precolumn, which resulted in a quasi-controlled variation of the retention time, 11−20 min. The back-exchange rate was measured and analyzed by means of a linear function of the retention time, $at_{rt} + b$, independently for each peptide.

Determination of Deuterium Incorporation. The level of deuteration, $D_{\%}$, was calculated according to (*24*)

$$D_{\%} = \frac{M_{HD}(t_{ex}) - M_{0\%}}{M_{100\%} - M_{0\%}} \times 100 \qquad (1)$$

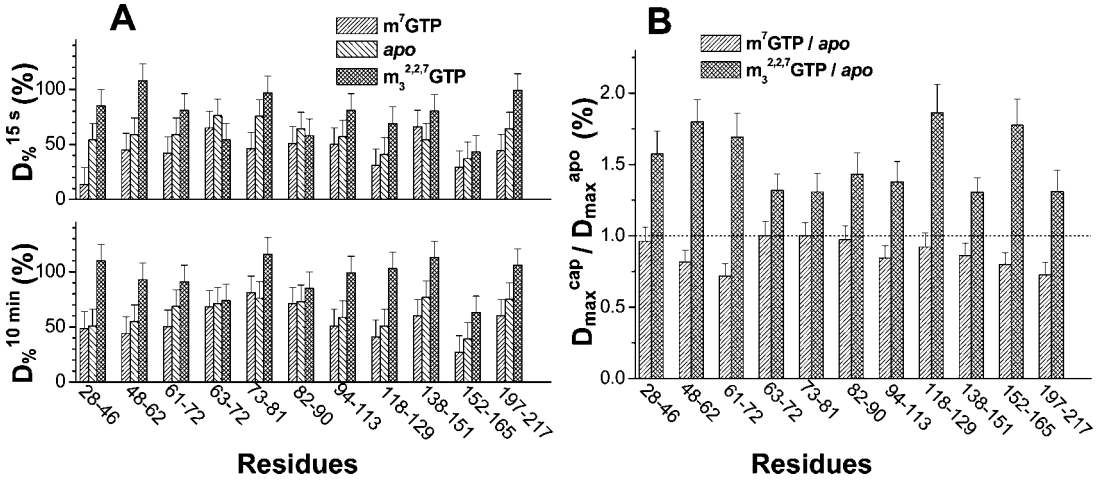

FIGURE 3: (A) Percentage of deuterium incorporation, $D_{\%}$, into different regions of *apo*- and cap-bound eIF4E after shorter, 15 s (top), and longer, 10 min (bottom), exchange time. $D_{\%}$ was calculated according to eq 3. (B) Maximal deuteration level of the cap-bound eIF4E in comparison with the *apo* form, $D_{max}^{cap}/D_{max}^{apo}$. D_{max} is a sum of all exchangeable amide hydrogens in all kinetic classes, detectable within the experimental time scale, and calculated according to eqs 4 and 5.

where $M_{HD}(t_{ex})$ is the weighted average of the mass peak distribution after the $^1H-^2H$ exchange time, t_{ex}, $M_{0\%}$ is the weighted average of the mass peak distribution of the nonexchanged peptide (control 1), and $M_{100\%}$ is the weighted average of the mass peak distribution corresponding to the completely exchanged peptide (control 2). The changes of peptide masses before and after maximal HDE determined directly from the raw data were in the range of 0.8−2.5 Da due to high back-exchange; hence a following correction was implemented.

The equation was modified to take into account back-exchange that occurred during the HPLC retention time, t_{rt}, bearing in mind that both M_{HD} and $M_{100\%}$ of each analyzed peptide have to be determined for the same retention time, and thus for the same delay, starting from pepsin digestion to the mass determination in the spectrometer:

$$D_{\%} = \frac{M_{HD}(t_{ex},t_{rt}) - M_{0\%}}{M_{100\%}(t_{rt}) - M_{0\%}} \times 100 \quad (2)$$

A retention time shift between the HPLC runs precluded direct measurements of $M_{100\%}(t_{rt})$. Measurements of deuterium incorporation for given t_{ex} were performed with the shortest retention time possible, in at least three independent series. The time dependence of the maximal number of the exchanged protons for each peptide, $M_{100\%}(t_{rt}) - M_{0\%}$, was approximated by a linear function of the retention time, $at_{rt} + b$, with the fitting parameters, a and b, derived from linear regression to the previously measured experimental data describing the back-exchange. Hence

$$D_{\%} = \frac{M_{HD}(t_{ex},t_{rt}) - M_{0\%}}{at_{rt} + b} \times 100 \quad (3)$$

The total number of deuterons, D, present in each particular peptide at time t_{ex} was calculated using a specific t_{rt} of that peptide, as follows:

$$D = \frac{M_{HD}(t_{ex},t_{rt}) - M_{0\%}}{at_{rt} + b} \times H_{amide} \quad (4)$$

where H_{amide} was the number of all amide protons belonging to the peptide bonds in the sequence.

Data Analysis. Numerical analyses were performed using OriginPro 7.5 (OriginLab Co.) and Prism 3.02 (GraphPad Software, Inc.). Kinetic parameters of amide deuteration were derived from nonlinear fitting of a multiexponential function to the data points calculated from eq 3 (Figures 1 and 4) or eq 4 (*42*):

$$D(t_{ex}) = \sum_i D_i(1 - e^{-k_i t_{ex}}) \quad (5)$$

where k_i are the rate constants and D_i are the numbers of protons exchanging at corresponding rates observable in the experimental time scale. A choice of the final model applied in the particular regression, i.e., the number and the kind of floating parameters related to different possible categories of amides, was determined on the basis of the statistical two-parameter Snedecor's F-test (*43*) with the significance level $P(\nu_1,\nu_2) = 0.1$. The selected model had the greatest possible number of floating parameters that led to the statistically important [$P(\nu_1,\nu_2) < 0.1$] improvement of the fit. For peptides that showed an immediate exchange, a monoexponential function with one floating parameter, D_1, and the fast rate constant, k_1, fixed as 30 min^{-1} (*30, 44*) proved to be statistically satisfactory. In some cases, two-parametric models were sufficient, and then two types of functions were possible, i.e., a monoexponential function with floating D_1 and k_1 or a two-exponential function with the fast rate, k_1, fixed as 30 min^{-1} and the slow rate, k_2, fixed as 0.1 min^{-1}, according to Mandell et al. (*30*) and Hoofnagle et al. (*31*), while D_1 and D_2 were free. A choice was then made directly on the basis of the absolute sums of squares. In remaining cases, two-exponential functions with either k_1 fixed as 30 min^{-1} and floating D_1, k_2, D_2 or with all floating parameters fit best. A three-exponential function with one rate fixed as either ≥30 min^{-1} or ≤0.1 min^{-1} did not improve the fits in any case.

Error Calculus. All reported errors were calculated according to propagation rules by the exact differential method (*45*). Total experimental errors of the data points (Figures 3 and 4) include both the uncertainty of a result of a single experiment, calculated from the uncertainties of all experimentally determined parameters that appear in eq 3, and the statistical scattering of the results obtained from different

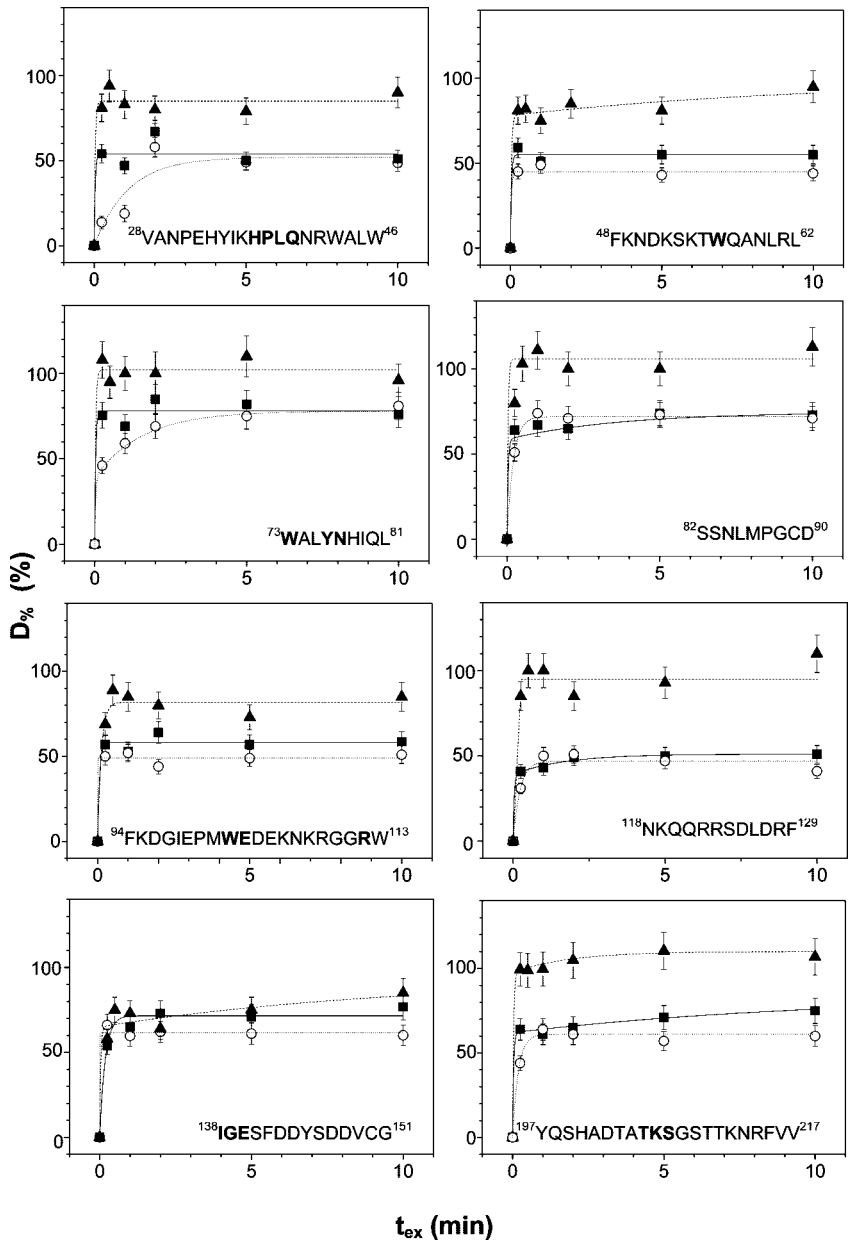

FIGURE 4: Kinetic traces of hydrogen–deuterium exchange for selected peptides derived from pepsin digestion of the eIF4E−m^{7}GTP complex (open circles), *apo*-eIF4E (filled squares), and the eIF4E−m$_3^{2,2,7}$GTP complex (filled triangles). Exponential curves were fitted according to eqs 3 and 5. Sequences and residue numbers of the peptides are listed as insets in each panel. Residues engaged in the cap or 4E-BP/eIF4G binding are marked in bold.

experimental series. Standard errors reported in tables (SEM) were calculated on the basis of numerical uncertainty resulting from the fitting.

RESULTS AND DISCUSSION

Deuteration of Whole eIF4E. The possibility of exchange of amide protons for deuterons is regulated by the local secondary structure, dynamics, and solvent accessibility which, in turn, can be influenced by interactions with ligands. We performed a series of HDE-MS experiments on murine eIF4E in the *apo* form and in the binary complexes with two cap analogues, m^{7}GTP (MMG-cap) or m$_3^{2,2,7}$GTP (TMG-cap). The MMG-cap analogue binds to eIF4E with the highest equilibrium association constant, K_{as}, of 10^8 M^{-1}, while the K_{as} value for m$_3^{2,2,7}$GTP is ~700-fold lower (*6*). We were able to selectively observe the changes of the intrinsic amide exchange rate constants, k_{ex}, in these eIF4E−cap complexes, since the association rate constant, k_a (*46*), for the electrostatically driven encounter (*6, 47*) of eIF4E with mononucleotide triphosphates ensured that k_a-[cap] $\geq 10^6$ min$^{-1} \gg k_{ex}$ at our exprimental conditions (*30*).

The results of HDE-MS experiments for all eIF4E forms are presented in Figure 1 and Table 1. In general, deuteration of eIF4E is rapid and is almost completed already after 5 min. Each protein form showed two classes of amides. The *apo* form had ~55 immediately exchanging amides with the fixed fast rate of 30 min^{-1} (*30*) and ~37 of those with an intermediate rate of ~4 min^{-1}. Slowly exchanging hydrogens were not detected. These results are in accord with previous findings that large regions of *apo*-eIF4E have a highly fluctuating (*7*) and partially disordered (*20*) structure.

Table 1: Overall Solvent Accessibility of Amide Hydrogens in eIF4E in the m^7GTP-, *apo*-, and $m_3^{2,2,7}$GTP-Bound Forms[a]

protein form	*D*	*k* (min^{-1})
m^7GTP complex	60.3 ± 1.4	30[b]
	14 ± 5	0.1[b]
apo	55 ± 30	30[b]
	37 ± 30	4 ± 3
$m_3^{2,2,7}$GTP complex	68 ± 3	30[b]
	49 ± 3	0.78 ± 0.10

[a] D, number of deuterons; *k*, corresponding exchange rate constant. Kinetic parameters of hydrogen–deuterium exchange were determined by nonlinear regression according to eqs 2 and 5. Experimental data were approximately corrected for back-exchange estimated as ~75%. [b] Values fixed as constant parameters of fitting (*30*).

By contrast, both protein–ligand complexes showed no intermediate class but slowly exchanging hydrogens were unambiguously detected instead, with the rate <1 min^{-1}, which suggests some ordering of the eIF4E structure upon binding of the ligands. The number of rapidly exchanging amide hydrogens was slightly reduced when eIF4E was complexed with the MMG-cap in comparison with the TMG−cap complex. This means that some residues, which are completely solvent accessible in the TMG−cap complex, are protected in the MMG−cap complex. The most interesting observation is that the total number of exchangeable amides was significantly greater in the eIF4E−TMG complex (117 ± 4) than in the eIF4E−MMG complex (69 ± 4) and even in the *apo* form (~90). This difference results from the large number of slowly exchanging amides that appear in the TMG−cap complex, which is greater by ~40 than that for the MMG-cap, while the number of fast backbone amides, completely exposed to the solvent, is similar in all protein forms, within the 95% confidence interval. The appearance of tens of additional slowly exchanging amide hydrogens suggests that some large parts of the protein interior, which are completely solvent-protected in the eIF4E−m^7GTP complex, become slightly solvent-accessible in eIF4E bound to $m_3^{2,2,7}$GTP. Hence, one can speculate that the overall protein conformation is influenced by the hypermethylated cap binding.

These observations prompted us to perform more detailed studies focused on local conformational changes, based on pepsin-generated peptides. However, the results obtained for the whole protein should not be quantitatively related to those determined from the pepsin cleavage experiments due to different experimental setup which rendered the correction for back-exchange of the undigested protein only approximate, while the corresponding corrections for the peptides were determined more precisely, as follows.

Improvements of HDE Methodology. Our HDE methodology included systematic corrections for back-exchange calculated for each individual peptide as well as unambiguous identification of the peptides on the basis of their retention times, similarly to the Griffin group (*48*). Our method was enriched by explicit visualization of the signals on 2D maps (HPLC retention time vs *m*/*z*, Figure 2C,F,G), which provided us with over 80% sequence coverage of both light and deuterated peptides.

To minimize back-exchange, the retention time was kept as short as possible. This caused a decrease in the quality of the peptide separation during the LC step and was compensated by using the 2D signal maps. However, the extent of back-exchange was very significant, up to 70–85% of the total initial value after 10 min on HPLC. A similarly high, 80% and 90% loss of deuterium after 10 and 20 min, respectively, was recently reported in systematic MS and NMR studies of amide hydrogen back-exchange in deuterated peptides (*49*). Application of LC was sometimes found to lead to back-exchange up to 60% (*50, 51*), and quite efficient back-exchange, up to 50%, was also detected even in such assays that minimized the time spent by peptides in H_2O by omitting the HPLC stage and using MALDI instead of ESI-MS (*29, 52, 53*). This indicates that systematic corrections for back-exchange, e.g., as proposed herein, should be applied in studies of proteins where conclusions are drawn from quantitative analysis based on the HDE data.

Since it was impossible to calculate the back-exchange level for each peptide theoretically, we performed a complete deuteration experiment for each analyzed peptide and determined a relationship of the back-exchange level of the amide protons on the controlled retention time, t_{rt}. The coefficients describing time-dependent back-exchange for each peptide are summarized in Table 2. The suitable values of *a* and *b* were then introduced into denominators of eqs 3 and 4 to recover the proper extent of peptide deuteration.

Peptide Identification. Pepsin digestion of eIF4E provided enough protein fragments to cover almost the whole protein sequence in a reproducible manner. The enzyme was found to be very efficient even at 1:1 enzyme-to-protein ratio during the short digestion times, <10 min. The identification of peptides by mass spectrometry allowed to determine the level of deuterium incorporation in various, well-defined parts of eIF4E and hence gave insight into the structure flexibility and solvent accessibility.

The signals of the exchanged peptides are generally lower than those of the corresponding peptides in the control samples either because of nonhomogeneous deuterium exchange that created several species for a given peptide (*54*) or due to insufficient signal-to-noise ratio resulting from the envelope broadening caused by the exchange (*55*). In addition, HDE can lead to overlapping of the mass peaks for the coeluting peptides. A set of useful pepsin-generated peptides of eIF4E (28–217) covered 81% of the sequence in the *apo* form and in the complex with m^7GTP and 75% in the complex with $m_3^{2,2,7}$GTP. We have chosen these 11 common peptides (Tables 2−4) that covered 75% of the eIF4E sequence in each form. Their masses were also determined after exchange in all eIF4E forms by localizing appropriate peaks in the signal maps (Figure 2). Among them, there were the peptide fragments that form both the cap-binding pocket, i.e., S1–S2 loop (residues 48–62), S3−S4 loop (residues 94–113), and β-fragment S5–S6 (residues 152–165), as well as the 4E-BP/eIF4G binding region, β-fragment S2 (residues 61–72), α-helix H2 (residues 73–81), and H6−S5 loop (residues 138–151) (Table 3, Figure 6). In particular, the analyzed peptide fragments contained two tryptophans (W56 and W102) and glutamic acid (E103) engaged in sandwich cation−π stacking and hydrogen bonding with the 7-methylguanosine moiety, arginines and lysines (R112, R157, K162, and K206) that stabilize the cap phosphate chain, and residues forming the 4E-BP/eIF4G binding site. Unfortunately, an important peptide in the 4E-BP/eIF4G binding region, ^{127}DRFWLETL^{134}, was hardly

Table 2: Parameters of Linear Regression for Back-Exchange in the Initially Fully Deuterated Pepsin-Generated eIF4E Peptides

residues	sequence	mass (Da)	*a*	*b*
28–46	VANPEHYIKHPLQNRWALW	2371.2	−0.13 ± 0.10	4.6 ± 1.5
48–62	FKNDKSKTWQANLRL	1848.0	−0.15 ± 0.10	4.3 ± 1.4
61–72	RLISKFDTVEDF	1468.8	−0.09 ± 0.01	2.8 ± 0.2
63–72	ISKFDTVEDF	1199.6	−0.04 ± 0.01	1.65 ± 0.12
73–81	WALYNHIQL	1156.6	−0.06 ± 0.02	2.5 ± 0.3
82–90	SSNLMPGCD	922.4	−0.04 ± 0.02	1.2 ± 0.3
94–113	FKDGIEPMWEDEKNKRGGRW	2477.2	−0.10 ± 0.03	3.6 ± 0.6
118–129	NKQQRRSDLDRF	1561.8	−0.06 ± 0.03	2.7 ± 0.2
138–151	IGESFDDYSDDVCG	1577.6	−0.14 ± 0.01	3.5 ± 0.2
152–165	AVVNVRAKGDKIAI	1452.9	−0.25 ± 0.21	4.9 ± 3.0
197–217	YQSHADTATKSGSTTKNRFVV	2297.2	−0.06 ± 0.02	2.98 ± 0.03

Table 3: Maximal Level, D_{max}/H_{amide}, of Deuterium Incorporation into Different Parts of m^7GTP-Bound, *apo*-, and $m_3^{2,2,7}$GTP-Bound eIF4E[a]

			D_{max}/H_{amide} (%)		
residues	function	secondary structure	m^7GTP	*apo*	$m_3^{2,2,7}$GTP
28–46		loop/*β*	52 ± 7	54 ± 3	85 ± 3
48–62	cap binding	loop/α	45 ± 1	55 ± 1	99 ± 11
61–72	4E-BP/eIF4Gbinding	*β*/α	51 ± 5	71 ± 6	120 ± 15
63–72	4E-BP/eIF4Gbinding	*β*/α	72 ± 1	72 ± 1	95 ± 6
73–81	4E-BP/eIF4Gbinding	α/turn	78 ± 5	78 ± 3	102 ± 3
82–90		loop	72 ± 1	74 ± 6	106 ± 2
94–113	cap binding	loop/turn	49 ± 1	58 ± 2	80 ± 3
118–129		α/turn/α	47 ± 2	51 ± 3	95 ± 3
138–151	4E-BP/eIF4Gbinding	α/*β*/α	62 ± 1	72 ± 2	94 ± 12
152–165	cap binding	*β*	32 ± 2	40 ± 1	71 ± 7
197–217	cap binding	*β*/α/*β*	61 ± 2	84 ± 4	110 ± 5

[a] D_{max} is a sum of all exchangeable hydrogens in all kinetic classes, detectable within the experimental time scale, and calculated according to eqs 4 and 5. The level of D_{max}/H_{amide} corresponds to the plateau in HDE kinetics (Figure 4, eqs 3 and 5).

Table 4: Kinetic Parameters of Hydrogen–Deuterium Exchange for Pepsin-Generated Peptides of m^7GTP-, *apo*-, and $m_3^{2,2,7}$GTP-Bound eIF4E[a]

	D and *k* (min^{-1})								
	m^7GTP			*apo*			$m_3^{2,2,7}$GTP		
residues	fast[b]	intermediate	slow[c]	fast[b]	intermediate	slow[c]	fast[b]	intermediate	slow[c]
28–46			*8.27 ± 1.13* *0.9 ± 0.4*	8.6 ± 0.5			13.6 ± 0.3		
48–62	6.33 ± 0.13			7.7 ± 0.2			11.0 ± 0.4		2.99 ± 1.12
61–72		5.61 ± 0.06 *7.0 ± 0.5*		6.1 ± 0.3		1.9 ± 0.7	10.4 ± 0.4		2.9 ± 1.3
63–72		6.53 ± 0.15 *9.0 ± 1.9*		6.50 ± 0.12			7.14 ± 0.12		1.4 ± 0.4
73–81	3.3 ± 0.2		*3.1 ± 0.2* *0.62 ± 0.11*	6.2 ± 0.2			8.12 ± 0.18		
82–89		5.06 ± 0.05 *4.9 ± 0.3*		4.4 ± 0.2		0.8 ± 0.3 *0.3 ± 0.3*		7.4 ± 0.2 *5.8 ± 0.9*	
94–113	8.9 ± 0.2			10.4 ± 0.3			14.4 ± 0.5		
118–129		5.2 ± 0.2 *4.3 ± 1.09*		4.3 ± 0.2		1.3 ± 0.2 *0.6 ± 0.2*	10.5 ± 0.4		
138–151	8.02 ± 0.13				9.3 ± 0.3 *5.5 ± 1.0*		8.5 ± 0.5		3.8 ± 1.6
152–165	4.2 ± 0.2				5.29 ± 0.13 *9.6 ± 2.4*		9.2 ± 0.5		
197–217		12.1 ± 0.3 *5.3 ± 0.7*		12.3 ± 0.2		4.4 ± 0.7	19.3 ± 0.5		2.5 ± 0.5 *0.5 ± 0.3*

[a] *D*, number of deuterons; *k*, corresponding exchange rate constant (in italics) for three kinetic categories of amides (fast, intermediate, and slow). Kinetic parameters were determined from the nonlinear regression according to eqs 4 and 5. [b] The fast rate constant was fixed as 30 min^{-1} (*30*). [c] The slow rate constant was fixed as 0.1 min^{-1} (*30, 31*), unless explicit values are indicated.

detectable by HPLC-MS in a positive ion mode due to strong hydrophobicity and negative charge of the peptide.

Deuteration Level and HDE Kinetics of Pepsin-Generated eIF4E Peptides. Analysis of HDE kinetics made it possible to determine a maximal level of peptide deuteration, D_{max}/H_{amide}, attainable within the experimental time scale, as well as to divide the exchangeable amides into three kinetic categories (*30, 31*). The results obtained from nonlinear data analysis are presented in Tables 3 and 4 and Figures 3 and 4. The parameters reflect differences in accessibility of the solvent molecules to various parts of the protein in each form.

In general, hydrogen–deuterium exchange kinetics is rapid for all peptides in each of the eIF4E forms. HDE-MS data show that association of m^7GTP leads to a decrease of the HDE level in all peptides (average exchange of 57%) in comparison with the *apo* form (65%), while binding of $m_3^{2,2,7}$GTP leads always to an elevated deuterium exchange (96%) (Table 3, Figures 3 and 4). This is in accordance with

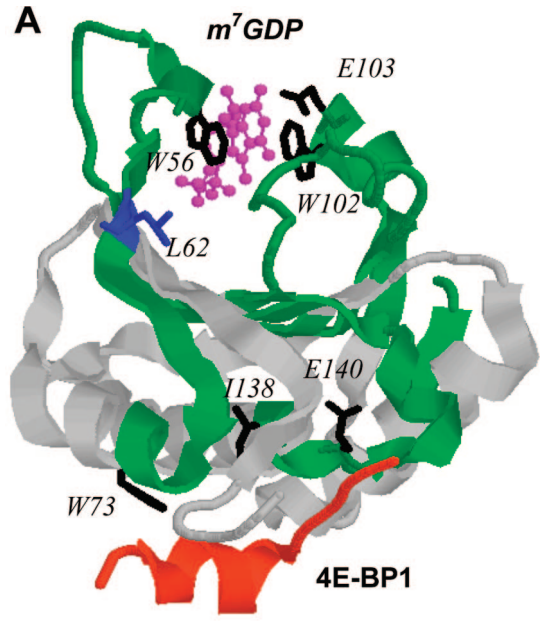

B

```
                    60          70
                    ----------  ---
 H.sapiens eIF4E    WQANL RLISKFDTVE DFW
H.musculus eIF4E    WQANL RLISKFDTVE DFW
 C.elegans IFE-3    WEDCL KMVSLFDTVE DFW
    A.suum IFE-3    WEDCL KQVAVFDTVE DFW
 C.elegans IFE-1    WEDRL KKVYTFNTVS EFW
 C.elegans IFE-5    WQDRL KKVYTFNTVP EFW
 C.elegans IFE-2    WEERL KNVKTFSSVG EFW
 C.elegans IFE-4    YASYV QPVGIMKSVE QFW
```

FIGURE 5: (A) X-ray structure of eIF4E (PDB id code 1EJ4 (*14*) in the complex with m^{7}GDP (magenta) and 4E-BP1 peptide fragment (red). Peptides with the largest changes between the *apo*- and m^{7}GTP-bound forms ($D_{max}^{cap}/D_{max}^{apo} < 0.9$) are shown in green (48–62, 61–72, 94–113, 138–151, 152–165, and 197–217). Some amino acids stabilizing the m^{7}G moiety (W56, W102, and E103) and 4E-BP1 (W73, I138, and E140) are marked in black. L62 that could putatively modulate the TMG cap binding is marked in blue. (B) Sequence alignments of eIF4E homologues (residues 56–73) from human (*60*), mouse (*61*), *C. elegans* (*62, 63*), and *A. suum* (*64*).

the estimates of the total amount of exchangeable amides obtained for the undigested protein that was 1.7-fold greater for the TMG−cap complex than for the MMG-cap (Table 1, Figure 1).

Several processes contribute to slowing the HDE in the cap-binding regions upon saturation with m^{7}GTP (Table 4). The number of rapidly ($k = 30$ min^{-1}) or moderately ($k \sim 10$ min^{-1}) exchanging amides is reduced by four in those peptides; 12 fast amides belonging to the C-terminal peptide (197–217) are slowed to ~ 5 min^{-1} in the m^{7}GTP complex, and 4 weakly exchangeable amides ($k = 0.1$ min^{-1}) become completely protected in the complex. Hence, according to the interpretation proposed by Mandell et al. (*30*), these changes can be partially attributed to simple shielding of the binding site by the tightly bound ligand and to ordering of the protein structure upon the cap binding (*7, 20, 21*).

Strikingly, the most significant changes in the HDE kinetics for *apo*- and m^{7}GTP-bound eIF4E are observed for the fragments which are not engaged in cap binding but contain amino acids responsible for interaction with 4E-BP or eIF4G (Figures 3, 4, and 5A, Tables 3 and 4). In the N-terminal fragment (28–46) that forms a kind of a "wrist" around which eIF4G forms a molecular "bracelet" (*56*), all amides that reveal immediate exchange ($k = 30$ min^{-1}) in the *apo* form are shifted to the slowest kinetic category ($k = 0.1$ min^{-1}) after m^{7}GTP binding. Six fast amides which belong to the next part of the 4E-BP/eIF4G binding site (61–72), containing residues that buttress the common 4E-BP/eIF4G helix (*14, 18, 56*), are slowed to ~ 7 min^{-1}, and two slow amides become hidden upon m^{7}GTP binding. In the W73-containing peptide (73–81), three of the six fast amides are markedly slowed to ~ 0.6 min^{-1}. In the acidic region of 138–151, one of the nine intermediate hydrogens ($k \sim 6$ min^{-1}) becomes buried while eight remaining become fully solvent accessible ($k = 30$ min^{-1}).

While the nature of the eIF4E conformational changes underlying the cap-binding enhancement in the presence of eIF4G has been studied exhaustively (*56*), our results suggest a possible submolecular mechanism by which the 5′ cap can modulate eIF4E recognition by eIF4G or 4E-BPs. Thus, association of eIF4E with the cap structure makes the cap-distal, 4E-BP/eIF4G binding surface to assume locally more compact shape suitable for tight interaction with the proteins. This proves a possibility of long-range conformational changes in outlying protein regions induced by specific binding of a small ligand.

Binding of $m_3^{2,2,7}$GTP makes the backbone of the entire protein much more solvent-accessible (Tables 3 and 4, Figures 3 and 4). In each peptide coming from eIF4E in the complex with $m_3^{2,2,7}$GTP, the number of immediately or moderately exchanging amides is significantly greater than in the *apo*-protein. The results seem to suggest that the majority of the eIF4E structure is influenced by binding of $m_3^{2,2,7}$GTP due to sterical hindrances caused by the additional two methyl groups at N^2 of the cap.

Interestingly, the HDE data made it possible to address the question, what eIF4E region could contribute most to the MMG vs TMG specificity of the mammalian protein? The comparison of two similar peptides, i.e., 61–72 and 63–72, reveals that the longer peptide is more sensitive to the presence of different cap analogues than the peptide shorter by two residues (Tables 3 and 4). This suggests that two amino acids belonging to the S2 β-sheet, R61 and L62, can play a role in discrimination between the MMG and TMG form of the cap. Sequence alignments of human and murine eIF4E with its five isoforms from *C. elegans* and eIF4E-3 from *Ascaris suum* show that the position corresponding to 62 in human eIF4E is taken by different types of residues in the proteins which are selective to the MMG-cap vs the proteins which exhibit affinity to both MMG and TMG cap (Figure 5B). The proteins specific to MMG have hydrophobic residues (L, M, or P), while those with the affinity to both the MMG- and TMG-cap possess residues with the amine group (Q, N, or K) here, which is capable of being a donor to a hydrogen bond. Putative contribution of these amino acids to the cap-binding process requires further studies by mutation analysis.

Conformational Differences between apo- and Cap-Bound eIF4E. Structure determination of *apo*-eIF4E by multidimensional NMR in solution (*21*) elucidated some conformational changes upon formation of complexes with m^{7}GDP by comparison with the crystallographic data (*15, 16*). The secondary structures of the *apo*- and the m^{7}GDP-bound forms are similar (Figure 6). Significant rearrangements occur in the cap-binding region. The fragment containing W56 moves

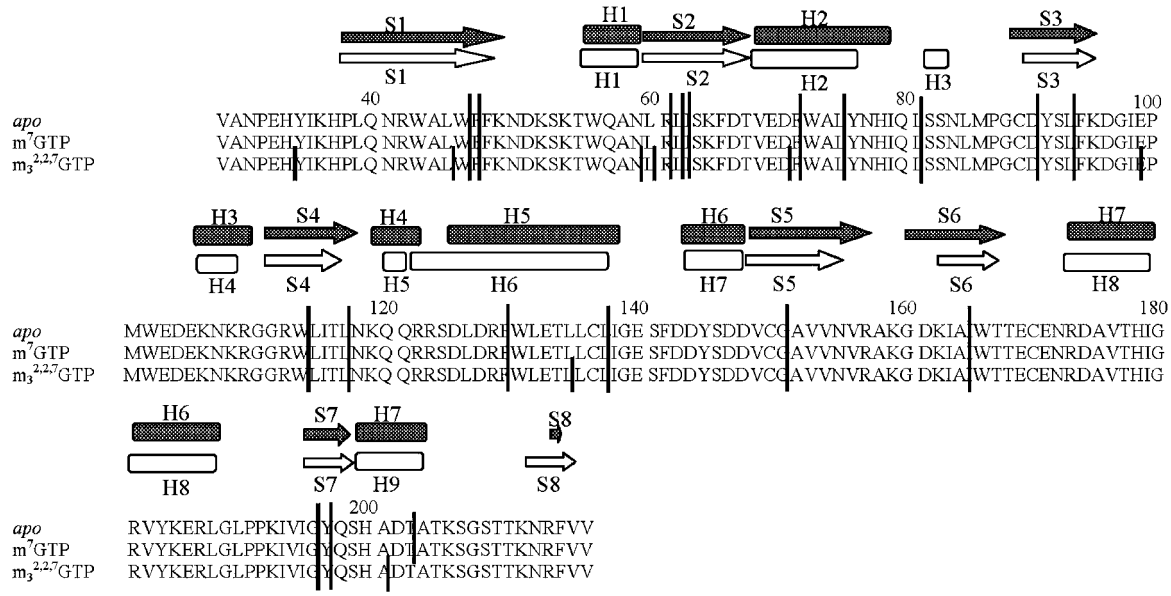

FIGURE 6: Comparison of secondary structure elements of *apo*-eIF4E (shaded, PDB id code 2GPQ (*21*)) with m^{7}GDP-bound eIF4E (plain, PDB id code 1EJ1 (*15*)). The secondary structure elements are represented schematically using DSSP parameters (*65*), β-sheets (S) as arrows and helices (H) as rectangles. The pepsin cleavage sites are marked with vertical black lines.

as a hinge without any changes in the secondary structure, while the region that contains W102 and E103 becomes more helical upon cap binding. The eIF4G/4E-BP binding site was found to have hampered dynamics (*21*). Our HDE results generally confirm these conclusions. However, we show further that the whole eIF4E backbone becomes much more solvent protected in a tight complex with m^{7}GTP. Additionally, we show that interaction with m^{7}GTP shifts the N-terminal tail into a more structured state. Together, the HDE data establish long-range cooperativity between distant eIF4E regions.

The HDE results directly show that formation of specific cap−eIF4E complexes causes significant stiffening of the eIF4E structure, as was postulated indirectly on the basis of our previous thermodynamic studies (*19*). We were also able to point out the specific protein regions that underwent an induced folding upon cap binding (*20*). In the light of our data it is not surprising that the cap binding enhances the eIF4E affinity for eIF4G/4E-BP (*18, 57, 58*) and changes the kinetics of eIF4G binding toward more rapid interaction (*20*) because the eIF4E dorsal surface is more compact when complexed with the cap. It is also clear now that specific cap binding yields such conformational changes in the N-terminal part that could be responsible for the observed protein disaggregation upon interaction with high-affinity cap analogues (*19*) and prevention from spontaneous degradation (*59*).

Opposite results were obtained for m$_3^{2,2,7}$GTP binding since an elevated solvent accessibility of the whole protein backbone was observed. Our results allow us to propose a binding model of the TMG cap to eIF4E. The additional methyl groups of TMG can prevent the W56-containing fragment from closing it up due to sterical effects, but the attempt to bind the cap tightly by cation$-\pi$ stacking interactions causes disturbance of the structure in other parts of the protein. Such structural disordering of the protein clearly explains a puzzling fact why m$_3^{2,2,7}$GTP binding to eIF4E is highly entropy-favorable at 20 °C, as opposed to other mRNA cap analogues (*7*).

Pepsin Cleavage Pattern. We have observed some differences in the cleavage sites of various eIF4E forms (Figure 6). The pepsin cleavage pattern for eIF4E is slightly changed if the protein is saturated to 99% with m$_3^{2,2,7}$GTP. New cleavage sites appear around W56 only for this complex. They are located just between residues L45−W46 and between residues N59−L60 and L60−R61. Hence, the pepsin cleavage pattern seems to confirm in the independent manner the above-mentioned conclusions drawn from HDE experiments that the W56-containing short helix could be crucial in discrimination between the MMG and TMG cap and that the neighborhood of R61 and L62 is mostly influenced by m$_3^{2,2,7}$GTP binding. As suggested by Volpon et al. (*21*), peptide fragment 48–62 can move as a hinge; hence the additional methyl groups can act as a sterical hindrance, preventing it from attaining the proper position upon binding to m$_3^{2,2,7}$GTP. The protein can then switch quickly between the "close" and "open" forms, and the sandwich stacking and hydrogen bonding cannot be formed properly. Again, this gives a clue for the explanation of low affinity of the hypermethylated cap to eIF4E.

CONCLUSIONS

The hydrogen–deuterium exchange method enabled us to monitor structural rearrangements of eIF4E upon binding of the mRNA 5′ cap analogues. Association of m^{7}GTP with eIF4E resulted in a marked decrease of the HDE level in all eIF4E peptide sequences in comparison with the *apo* form. This indicates that the whole protein structure becomes less solvent-accessible, which can reflect a partial unfolded-to-folded transition. The most distinct finding is that, besides the cap-binding pocket, the region which is highly influenced by association with the MMG-cap belongs to the dorsal eIF4G/4E-BP binding site. On the other hand, the eIF4E backbone in the complex with m$_3^{2,2,7}$GTP is much more solvent-accessible than in the *apo* form. This structural destabilization would make the eIF4E−m$_3^{2,2,7}$GTP complex even more difficult to study by NMR or X-ray techniques

than the *apo*-protein, and hydrogen–deuterium exchange combined with mass spectrometry seems to be one of a few methods to handle such a dynamic phenomena.

ACKNOWLEDGMENT

We are indebted to the reviewers for exceptionally kind and helpful advice, Prof. Nahum Sonenberg for providing the plasmid of murine eIF4E, and Prof. Danek Elbaum and Dr. Joanna Trylska for critical reading of the manuscript.

REFERENCES

1. Prevot, D., Darlix, J. L., and Ohlmann, T. (2003) Conducting the initiation of protein synthesis: the role of eIF4G. *Biol. Cell 95*, 141–156.
2. Gingras, A. C., Raught, B., and Sonenberg, N. (1999) eIF4 initiation factors: effectors of mRNA recruitment to ribosomes and regulators of translation. *Annu. Rev. Biochem. 68*, 913–963.
3. Zorio, D. A., Cheng, N. N., Blumenthal, T., and Spieth, J. (1994) Operons as a common form of chromosomal organization in *C. elegans*. *Nature 372*, 270–272.
4. Keiper, B. D., Lamphear, B. J., Deshpande, A. M., Jankowska-Anyszka, M., Aamodt, E. J., Blumenthal, T., and Rhoads, R. E. (2000) Functional characterization of five eIF4E isoforms in *Caenorhabditis elegans*. *J. Biol. Chem. 275*, 10590–10596.
5. Stachelska, A., Wieczorek, Z., Ruszczynska, K., Stolarski, R., Pietrzak, M., Lamphear, B. J., Rhoads, R. E., Darzynkiewicz, E., and Jankowska-Anyszka, M. (2002) Interaction of three *Caenorhabditis elegans* isoforms of translation initiation factor eIF4E with mono- and trimethylated mRNA 5′ cap analogues. *Acta Biochim. Pol. 49*, 671–682.
6. Niedzwiecka, A., Marcotrigiano, J., Stepinski, J., Jankowska-Anyszka, M., Wyslouch-Cieszynska, A., Dadlez, M., Gingras, A. C., Mak, P., Darzynkiewicz, E., Sonenberg, N., Burley, S. K., and Stolarski, R. (2002) Biophysical studies of eIF4E cap-binding protein: recognition of mRNA 5′ cap structure and synthetic fragments of eIF4G and 4E-BP1 proteins. *J. Mol. Biol. 319*, 615–635.
7. Niedzwiecka, A., Darzynkiewicz, E., and Stolarski, R. (2004) Thermodynamics of mRNA 5′ cap binding by eukaryotic translation initiation factor eIF4E. *Biochemistry 43*, 13305–13317.
8. Duncan, R., Milburn, S. C., and Hershey, J. W. (1987) Regulated phosphorylation and low abundance of HeLa cell initiation factor eIF-4F suggest a role in translational control. Heat shock effects on eIF-4F. *J. Biol. Chem. 262*, 380–388.
9. Raught, B., and Gingras, A. C. (1999) eIF4E activity is regulated at multiple levels. *Int. J. Biochem. Cell Biol. 31*, 43–57.
10. Joshi, B., Cai, A. L., Keiper, B. D., Minich, W. B., Mendez, R., Beach, C. M., Stepinski, J., Stolarski, R., Darzynkiewicz, E., and Rhoads, R. E. (1995) Phosphorylation of eukaryotic protein synthesis initiation factor 4E at Ser-209. *J. Biol. Chem. 270*, 14597–14603.
11. Zuberek, J., Wyslouch-Cieszynska, A., Niedzwiecka, A., Dadlez, M., Stepinski, J., Augustyniak, W., Gingras, A. C., Zhang, Z., Burley, S. K., Sonenberg, N., Stolarski, R., and Darzynkiewicz, E. (2003) Phosphorylation of eIF4E attenuates its interaction with mRNA 5′ cap analogs by electrostatic repulsion: intein-mediated protein ligation strategy to obtain phosphorylated protein. *RNA 9*, 52–61.
12. Richter, J. D., and Sonenberg, N. (2005) Regulation of cap-dependent translation by eIF4E inhibitory proteins. *Nature 433*, 477–480.
13. Imataka, H., Gradi, A., and Sonenberg, N. (1998) A newly identified N-terminal amino acid sequence of human eIF4G binds poly(A)-binding protein and functions in poly(A)-dependent translation. *EMBO J. 17*, 7480–7489.
14. Marcotrigiano, J., Gingras, A. C., Sonenberg, N., and Burley, S. K. (1999) Cap-dependent translation initiation in eukaryotes is regulated by a molecular mimic of eIF4G. *Mol. Cell 3*, 707–716.
15. Marcotrigiano, J., Gingras, A. C., Sonenberg, N., and Burley, S. K. (1997) Cocrystal structure of the messenger RNA 5′ cap-binding protein (eIF4E) bound to 7-methyl-GDP. *Cell 89*, 951–961.
16. Tomoo, K., Shen, X., Okabe, K., Nozoe, Y., Fukuhara, S., Morino, S., Ishida, T., Taniguchi, T., Hasegawa, H., Terashima, A., Sasaki, M., Katsuya, Y., Kitamura, K., Miyoshi, H., Ishikawa, M., and Miura, K. (2002) Crystal structures of 7-methylguanosine 5′-triphosphate (m(7)GTP)- and P(1)-7-methylguanosine-P(3)-adenosine-5′, 5′-triphosphate (m(7)GpppA)-bound human full-length eukaryotic initiation factor 4E: biological importance of the C-terminal flexible region. *Biochem. J. 362*, 539–544.
17. Matsuo, H., Li, H., McGuire, A. M., Fletcher, C. M., Gingras, A. C., Sonenberg, N., and Wagner, G. (1997) Structure of translation factor eIF4E bound to m7GDP and interaction with 4E-binding protein. *Nat. Struct. Biol. 4*, 717–724.
18. Tomoo, K., Matsushita, Y., Fujisaki, H., Abiko, F., Shen, X., Taniguchi, T., Miyagawa, H., Kitamura, K., Miura, K., and Ishida, T. (2005) Structural basis for mRNA cap-binding regulation of eukaryotic initiation factor 4E by 4E-binding protein, studied by spectroscopic, X-ray crystal structural, and molecular dynamics simulation methods. *Biochim. Biophys. Acta 1753*, 191–208.
19. Niedzwiecka, A., Darzynkiewicz, E., and Stolarski, R. (2005) Thermodynamics and conformational changes related to binding of eIF4E protein to mRNA 5 cap. *J. Phys.: Condens. Matter 17*, 1483–1494.
20. von der Haar, T., Oku, Y., Ptushkina, M., Moerke, N., Wagner, G., Gross, J. D., and McCarthy, J. E. (2006) Folding transitions during assembly of the eukaryotic mRNA cap-binding complex. *J. Mol. Biol. 356*, 982–992.
21. Volpon, L., Osborne, M. J., Topisirovic, I., Siddiqui, N., and Borden, K. L. (2006) Cap-free structure of eIF4E suggests a basis for conformational regulation by its ligands. *EMBO J. 25*, 5138–5149.
22. Mann, M., Hendrickson, R. C., and Pandey, A. (2001) Analysis of proteins and proteomes by mass spectrometry. *Annu. Rev. Biochem. 70*, 437–473.
23. van den Heuvel, R. H., and Heck, A. J. R. (2004) Native protein mass spectrometry: from intact oligomers to functional machineries. *Curr. Opin. Chem. Biol. 8*, 519–526.
24. Zhang, Z., and Smith, D. L. (1993) Determination of amide hydrogen exchange by mass spectrometry: a new tool for protein structure elucidation. *Protein Sci. 2*, 522–531.
25. Engen, J. R., and Smith, D. L. (2000) Investigating the higher order structure of proteins. Hydrogen exchange, proteolytic fragmentation, and mass spectrometry. *Methods Mol. Biol. 146*, 95–112.
26. Maier, C. S., and Deinzer, M. L. (2005) Protein conformations, interactions, and H/D exchange. *Biol. Mass Spectrom. 402*, 312–360.
27. Hamuro, Y., Coales, S. J., Southern, M. R., Nemeth-Cawley, J. F., Stranz, D. D., and Griffin, P. R. (2003) Rapid analysis of protein structure and dynamics by hydrogen/deuterium exchange mass spectrometry. *J. Biomol. Technol. 14*, 171–182.
28. Englander, S. W. (2006) Hydrogen exchange and mass spectrometry: A historical perspective. *J. Am. Soc. Mass Spectrom. 17*, 1481–1489.
29. Mandell, J. G., Falick, A. M., and Komives, E. A. (1998) Identification of protein-protein interfaces by decreased amide proton solvent accessibility. *Proc. Natl. Acad. Sci. U.S.A. 95*, 14705–14710.
30. Mandell, J. G., Baerga-Ortiz, A., Akashi, S., Takio, K., and Komives, E. A. (2001) Solvent accessibility of the thrombin-thrombomodulin interface. *J. Mol. Biol. 306*, 575–589.
31. Hoofnagle, A. N., Resing, K. A., Goldsmith, E. J., and Ahn, N. G. (2001) Changes in protein conformational mobility upon activation of extracellular regulated protein kinase-2 as detected by hydrogen exchange. *Proc. Natl. Acad. Sci. U.S.A. 98*, 956–961.
32. Lam, T. T., Lanman, J. K., Emmett, M. R., Hendrickson, C. L., Marshall, A. G., and Prevelige, P. E. (2002) Mapping of protein: protein contact surfaces by hydrogen/deuterium exchange, followed by on-line high-performance liquid chromatography-electrospray ionization Fourier-transform ion-cyclotron-resonance mass analysis. *J. Chromatogr. A 982*, 85–95.
33. Wang, F., Scapin, G., Blanchard, J. S., and Angeletti, R. H. (1998) Substrate binding and conformational changes of *Clostridium glutamicum* diaminopimelate dehydrogenase revealed by hydrogen/deuterium exchange and electrospray mass spectrometry. *Protein Sci. 7*, 293–299.
34. Careri, M., Elviri, L., Mangia, A., Zagnoni, I., Torta, F., Cavazzini, D., and Rossi, G. L. (2006) Mass spectrometry techniques for detection of ligand-dependent changes in the conformational flexibility of cellular retinol-binding protein type I localized by hydrogen/deuterium exchange. *Rapid Commun. Mass Spectrom. 20*, 1973–1980.
35. Jankowska, M., Stepinski, J., Stolarski, R., and Darzynkiewicz, E. (1993) Synthesis and Properties of New NH2 and N7 Substituted

GMP and GTP 5′-mRNA Cap Analogues. *Collect. Czech. Chem. Commun. 58*, 138–141.
36. Darzynkiewicz, E., Ekiel, I., Tahara, S. M., Seliger, L. S., and Shatkin, A. J. (1985) Chemical synthesis and characterization of 7-methylguanosine cap analogs. *Biochemistry 24*, 1701–1707.
37. Edery, I., Altmann, M., and Sonenberg, N. (1988) High-level synthesis in *Escherichia coli* of functional cap-binding eukaryotic initiation factor eIF-4E and affinity purification using a simplified cap-analog resin. *Gene 74*, 517–525.
38. Zhang, Y. (1995) Protein and peptide structure and interactions studied by hydrogen exchange and NMR, Ph.D. Thesis, University of Pennsylvania, Philadelphia (http://www.fccc.edu/research/labs/roder/sphere/sphere.html).
39. Englander, S. W., and Kallenbach, N. R. (1983) Hydrogen exchange and structural dynamics of proteins and nucleic acids. *Q. Rev. Biophys. 16*, 521–655.
40. Bai, Y., Milne, J. S., Mayne, L., and Englander, S. W. (1993) Primary structure effects on peptide group hydrogen exchange. *Proteins 17*, 75–86.
41. Perkins, D. N., Pappin, D. J., Creasy, D. M., and Cottrell, J. S. (1999) Probability-based protein identification by searching sequence databases using mass spectrometry data. *Electrophoresis 20*, 3551–3567.
42. Berger, A., and Linderstrom-Lang, K. (1957) Deuterium exchange of poly-DL-alanine in aqueous solution. *Arch. Biochem. Biophys. 69*, 106–118.
43. Snedecor, G., and Cochran, W. G. (1989) *Statistical Methods*, Iowa State University Press, Ames, IA.
44. Gemmecker, G., Jahnke, W., and Kessler, R. (1993) Measurement of Fast Proton Exchange Rates in Isotopically Labeled Compounds. *J. Am. Chem. Soc. 115*, 11620–11621.
45. Taylor, J. R. (1982) *An Introduction to Error Analysis*, Oxford University Press, Oxford, U.K.
46. Blachut-Okrasinska, E., Bojarska, E., Stepinski, J., and Antosiewicz, J. M. (2007) Kinetics of binding the mRNA cap analogues to the translation initiation factor eIF4E under second-order reaction conditions. *Biophys. Chem. 129*, 289–297.
47. Blachut-Okrasinska, E., Bojarska, E., Niedzwiecka, A., Chlebicka, L., Darzynkiewicz, E., Stolarski, R., Stepinski, J., and Antosiewicz, J. M. (2000) Stopped-flow and Brownian dynamics studies of electrostatic effects in the kinetics of binding of 7-methyl-GpppG to the protein eIF4E. *Eur. Biophys. J. 29*, 487–498.
48. Pascal, B. D., Chalmers, M. J., Busby, S. A., Mader, C. C., Southern, M. R., Tsinoremas, N. F., and Griffin, P. R. (2007) The Deuterator: software for the determination of backbone amide deuterium levels from H/D exchange MS data. *BMC Bioinf. 8*, 156.
49. Feng, L. M., Orlando, R., and Prestegard, J. H. (2006) Amide proton back-exchange in deuterated peptides: Applications to MS and NMR analyses. *Anal. Chem. 78*, 6885–6892.
50. Ehring, H. (1999) Hydrogen exchange/electrospray ionization mass spectrometry studies of structural features of proteins and protein/protein interactions. *Anal. Biochem. 267*, 252–259.
51. Wang, F., Blanchard, J. S., and Tang, X. J. (1997) Hydrogen exchange/electrospray ionization mass spectrometry studies of substrate and inhibitor binding and conformational changes of *Escherichia coli* dihydrodipicolinate reductase. *Biochemistry 36*, 3755–3759.
52. Croy, C. H., Koeppe, J. R., Bergqvist, S., and Komives, E. A. (2004) Allosteric changes in solvent accessibility observed in thrombin upon active site occupation. *Biochemistry 43*, 5246–5255.
53. Sabo, T. M., Farrell, D. H., and Maurer, M. C. (2006) Conformational analysis of gamma′ peptide (410−427) interactions with thrombin anion binding exosite II. *Biochemistry 45*, 7434–7445.
54. Cravello, L., Lascoux, D., and Forest, E. (2003) Use of different proteases working in acidic conditions to improve sequence coverage and resolution in hydrogen/deuterium exchange of large proteins. *Rapid Commun. Mass Spectrom. 17*, 2387–2393.
55. Hughes, C. A., Mandell, J. G., Anand, G. S., Stock, A. M., and Komives, E. A. (2001) Phosphorylation causes subtle changes in solvent accessibility at the interdomain interface of methylesterase CheB. *J. Mol. Biol. 307*, 967–976.
56. Gross, J. D., Moerke, N. J., von der Haar, T., Lugovskoy, A. A., Sachs, A. B., McCarthy, J. E., and Wagner, G. (2003) Ribosome loading onto the mRNA cap is driven by conformational coupling between eIF4G and eIF4E. *Cell 115*, 739–750.
57. von der Haar, T., Gross, J. D., Wagner, G., and McCarthy, J. E. (2004) The mRNA cap-binding protein eIF4E in post-transcriptional gene expression. *Nat. Struct. Mol. Biol. 11*, 503–511.
58. Miyoshi, H., Youtani, T., Ide, H., Hori, H., Okamoto, K., Ishikawa, M., Wakiyama, M., Nishino, T., Ishida, T., and Miura, K. (1999) Binding analysis of *Xenopus laevis* translation initiation factor 4E (eIF4E) in initiation complex formation. *J. Biochem. (Tokyo) 126*, 897–904.
59. Tomoo, K., Shen, X., Okabe, K., Nozoe, Y., Fukuhara, S., Morino, S., Sasaki, M., Taniguchi, T., Miyagawa, H., Kitamura, K., Miura, K., and Ishida, T. (2003) Structural features of human initiation factor 4E studied by X-ray crystal analyses and molecular dynamics simulations. *J. Mol. Biol. 328*, 365–383.
60. Rychlik, W., Domier, L. L., Gardner, P. R., Hellmann, G. M., and Rhoads, R. E. (1987) Amino acid sequence of the mRNA cap-binding protein from human tissues. *Proc. Natl. Acad. Sci. U.S.A. 84*, 945–949.
61. Altmann, M., Muller, P. P., Pelletier, J., Sonenberg, N., and Trachsel, H. (1989) A mammalian translation initiation factor can substitute for its yeast homologue in vivo. *J. Biol. Chem. 264*, 12145–12147.
62. Jankowska-Anyszka, M., Lamphear, B. J., Aamodt, E. J., Harrington, T., Darzynkiewicz, E., Stolarski, R., and Rhoads, R. E. (1998) Multiple isoforms of eukaryotic protein synthesis initiation factor 4E in *Caenorhabditis elegans* can distinguish between mono- and trimethylated mRNA cap structures. *J. Biol. Chem. 273*, 10538–10542.
63. Keiper, B. D., Lamphear, B. J., Deshpande, A. M., Jankowska-Anyszka, M., Aamodt, E. J., Blumenthal, T., and Rhoads, R. E. (2000) Functional characterization of five eIF4E isoforms in *Caenorhabditis elegans*. *J. Biol. Chem. 275*, 10590–10596.
64. Lall, S., Friedman, C. C., Jankowska-Anyszka, M., Stepinski, J., Darzynkiewicz, E., and Davis, R. E. (2004) Contribution of trans-splicing 5′ -leader length, cap-poly(A) synergism, and initiation factors to nematode translation in an *Ascaris suum* embryo cell-free system. *J. Biol. Chem. 279*, 45573–45585.
65. Kabsch, W., and Sander, C. (1983) Dictionary of protein secondary structure: pattern recognition of hydrogen-bonded and geometrical features. *Biopolymers 22*, 2577–2637.

BI701168Z